

1 **Predicting morphological changes along a macrotidal coastline Using a Two-Stage**  
2 **Machine Learning Model**

3 **Pavitra Kumar<sup>1\*</sup> and Nicoletta Leonardi<sup>1</sup>**

4 <sup>1</sup>Department of Geography and Planning, School of Environmental Sciences, University of  
5 Liverpool, Chatham Street, Liverpool, L69 7ZT, UK

6 \* Corresponding Author: [pavitra.kumar@liverpool.ac.uk](mailto:pavitra.kumar@liverpool.ac.uk)

7 **Abstract:** Within the context of climate change, understanding and predicting coastal change  
8 is of the foremost importance to protect coastal communities and coastal assets. This study  
9 analyzes field data from 125 locations along the Morecambe coastline, consisting of beach  
10 transects collected twice a year for more than a decade (2007 to 2022). To model the  
11 sediment volume changes observed along the Morecambe coastline, this study proposes a  
12 two-stage machine learning model that incorporates beach behavior classification and deep  
13 learning techniques to predict changes in sediment volumes along coastal environments. The  
14 first stage of the model, developed using a random forest classifier, classifies beach behavior  
15 into four categories: eroding, accreting, stable, or undergoing short-term fluctuations. The  
16 second stage of the model developed using LSTM and sequence-to-sequence models, uses  
17 the output of the first stage to predict the available sediment volume after erosion/accretion.  
18 LSTM model achieved a testing regression of 0.9961 for one-step-ahead (6 months)  
19 predictions of sediment volume time series, while sequence-to-sequence model achieved the  
20 testing regression of 0.9950 for three-time-ahead (1.5 years) predictions and 0.9916 for ten-  
21 time-step-ahead (5 years) prediction.

22 **Plain Language Summary:** This study investigates how coastlines change over time,  
23 especially as the climate changes. We focused on the Morecambe Bay in England and  
24 analyzed data collected over 16 years from 2007 to 2022. Artificial intelligence models were

25 developed that learn from beach data to predict if a beach will erode (wash away), grow  
26 bigger, or stay the same. These models work in two steps: first, it figures out if the beach is  
27 eroding (wearing away), growing, staying the same, or changing in small bursts. Then, it uses  
28 that information to predict how much sediment a particular beach location will be there in 6  
29 months, 1.5 years, or even 5 years from now. These models are capable of accurately  
30 predicting beach behavior and sediments available, especially for short-term predictions. This  
31 information can help protect coastal towns and areas from the effects of climate change.

32 **Keywords:** Sediment volume; Morecambe Bay; Two-stage modeling; Random Forest;  
33 LSTM; Sequence-to-sequence

#### 34 **1. Introduction**

35 Dynamic coastal processes continuously shape the coastline and understanding  
36 coastal dynamics is important to protect coastal communities and coastal infrastructures.  
37 Waves, tidal energy and sediment availability determine sediment transport and  
38 morphological variations but anthropogenic activities can also accelerate the rate of coastline  
39 change (Prasad & Kumar, 2014; van Rijn, 2011; Williams et al., 2018). Over the years, more  
40 and more infrastructures have been built along the coastline. Coastal erosion causes the  
41 coastline to retreat inland. The removal of sediments from infrastructure locations can expose  
42 their foundations, reducing their strength and stability, and making them unsafe. With sea  
43 level rise and changes in storms activity, there is increased uncertainty about the risk of  
44 erosion, flooding and on whether the project lifetime of these infrastructures will prove  
45 adequate to withstand the challenges posed by climate change.

46 Several soft nourishment and hard structures are designed to address coastal erosion  
47 problems. Soft nourishment includes, for instance, shoreface nourishment (beach fills)  
48 (Kumar & Leonardi, 2023b, 2024a) and submerged reefs (Harris, 2012), while hard structures  
49 include groins (Lima et al., 2020), detached breakwaters (Browder et al., 2015), seawalls

50 (Betzold & Mohamed, 2017), and revetments (Crawford et al., 2020). To be effective, these  
51 engineering solutions must be installed at identified vulnerable locations. Historic erosion and  
52 deposition data as well as predictive models can be used to identify such locations,  
53 specifically those that can be classified as having long-term chronic erosion or short-term  
54 fluctuating erosion trends. For instance, if an area of interest experiences substantial sediment  
55 loss over 5-10 years, it can be considered to have long-term chronic erosion and thus requires  
56 erosion protection measures (van Rijn, 2011).

57 Machine Learning and predictive models such as artificial neural networks (ANNs)  
58 can be useful for nonlinear forecasting of coastal change (Kumar and Leonardi, 2023 a, b).  
59 These can be especially helpful when long-term morphodynamical models are not available  
60 or prove to be too computationally expensive. Historic data, whether from remote sensing or  
61 direct field campaigns can also be used to feed into the ANN models and identify erosion  
62 prone areas to support coastal management.

63 ANN models are information processing systems modelled on the structure of the  
64 human brain (Anctil et al., 2009; Sharma et al., 2003) and effective in dealing with  
65 nonlinearities (Farzad & El-Shafie, 2017) and have been successfully applied to other coastal  
66 engineering problems. ANN models can learn the nonlinear relationships between the  
67 different variables that influence coastal erosion, making them well-suited for modeling this  
68 complex process. ANN models can even learn dependencies that process-based models fail to  
69 capture. Several researchers have developed models to predict coastal erosion, including  
70 Peponi et al. (2019), Corbella and Stretch (2012) and Adamo et al. (2014). Peponi et al.  
71 (2019) integrated geographic information systems (GIS) with ANN to predict erosion-prone  
72 areas at the coastal zones of Costa da Caparica in Lisbon, Portugal, in the near future. They  
73 mainly considered anthropogenic inputs from GIS, such as the number of residents, land  
74 cover, number of households, and vegetated and non-vegetated areas, to predict erosion-

75 prone areas using ANN. Corbella and Stretch (2012) and Adamo et al. (2014) used process-  
76 based models to estimate coastal erosion. Corbella and Stretch (2012) used the SBEACH,  
77 XBEACH, and Time Convolution models to estimate coastal erosion trends at coastal areas  
78 of Durban, South Africa. Adamo et al. (2014) used directional wave spectrum and direction  
79 of wave propagation to estimate coastal erosion and used this it to estimate shoreline change.

80 This study proposes a combination of two prediction models to classify beach profiles  
81 based on their trends in morphological changes and to predict time series of morphological  
82 trends. Specifically, the objectives of this study are: 1) Utilizing high-quality field  
83 measurements from Morecambe Bay coastline, this study aims to harness real-time beach  
84 transect data for a comprehensive analysis. The primary goal is to construct a robust random  
85 forest classifier model that can accurately predict the long-term behavior of the coastline,  
86 categorizing it into erosion, accretion, stability, or short-term erosion fluctuation. 2) Focusing  
87 on the significant field measurements, this research seeks to advance predictive capabilities  
88 by developing a cutting-edge Long Short-Term Memory (LSTM) and sequence-to-sequence  
89 model. The central objective is to forecast the volume of sediment erosion or accretion at  
90 specific locations, further enhancing our ability to comprehend and anticipate coastal  
91 morphological changes.

92 Continuous field campaigns were conducted from 2007 to 2022 to collect beach  
93 profiles using GS16 Leica antenna and a Leica CS20 handset at 125 locations along  
94 Morecambe Bay. Simulation data, including coastal parameters such as wave height, wave  
95 direction, wave velocity, and coastline composition are obtained from a hydrodynamic model  
96 built using Delft3D and were fed along with historical data into the ANN models. The  
97 manuscript is organized as follows: After presenting the study site, the methodology section  
98 details the field data collection methods, hydrodynamic modeling techniques, machine  
99 learning models employed, and performance criteria used to evaluate the models'

100 effectiveness. The results section then presents the analysis of the gathered field data and  
101 model performance. Following this, the discussion section delves into the literature on  
102 coastline change in Morecambe Bay and explores the applicability of the developed models  
103 in this context. Finally, the conclusion section summarizes the study, highlighting key  
104 findings and implications.

## 105 **2. Study Site**

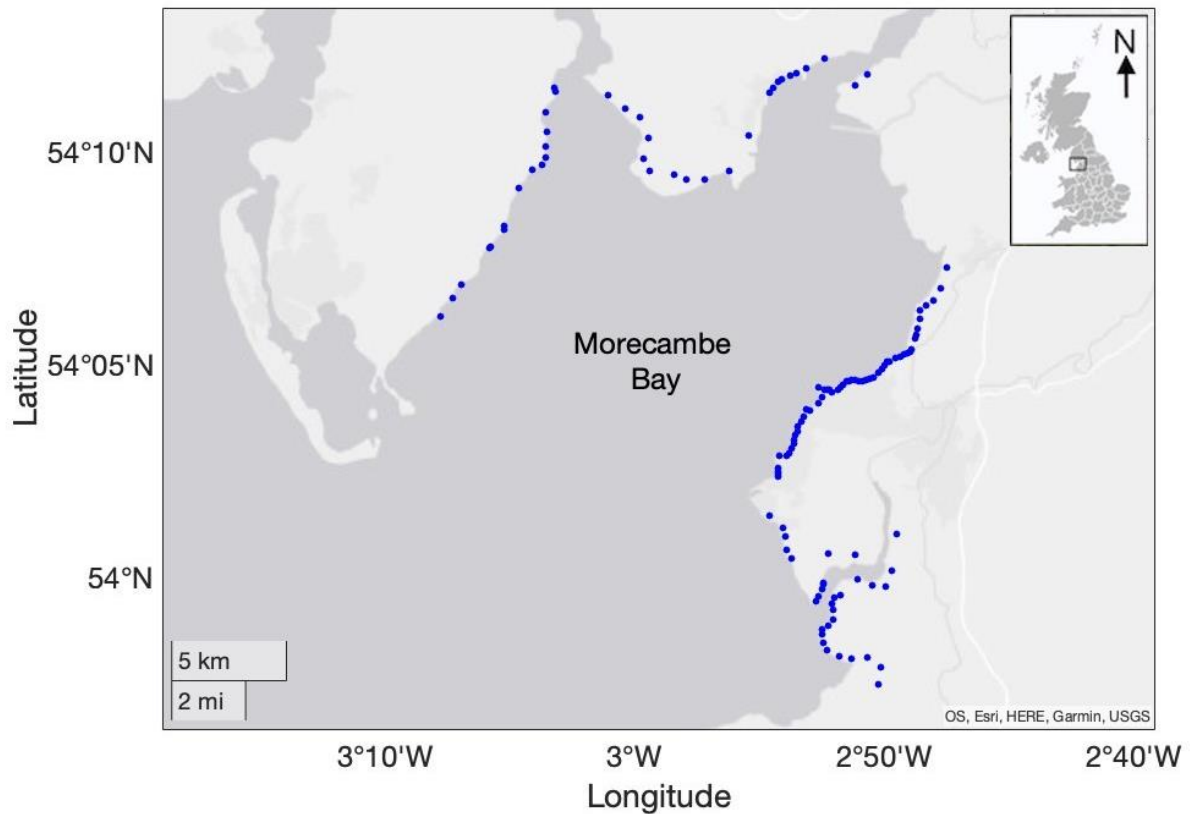
106 Morecambe Bay, a macrotidal embayment in northwest England, is the test case of  
107 this study. Its shoreline is mostly covered in fine sand, and the bay opens southwest into the  
108 Irish Sea (Mason et al., 2010). Intertidal zones, especially sandbanks and subtidal channels,  
109 are highly susceptible to change, and these changes can be observed even within a single  
110 season. The fetch length is constrained by landmasses such as Ireland and the Isle of Man. As  
111 a result, significant wave heights at the bay mouth reach up to 2 meters for only about 10% of  
112 the year, remaining around 0.5 meters for the rest of the year. Morecambe Bay has a large  
113 ordinary spring tidal range of approximately 8.2 meters and its subtidal channels experience  
114 maximum spring tide velocities of about 1.5 meters per second (Mason et al., 2010). During  
115 the 1991–2007 study period, Mason et al. (2010) found that the bay experienced significant  
116 sediment movement from below mean sea level to above mean sea level. This erosion and  
117 accretion caused the mudflat to retreat towards the landmass. Due to its dynamic behavior  
118 and significant sediment movement, this bay was selected for this study.

## 119 **3. Methodology**

### 120 **3.1 Field Data**

121 Sefton Council (Sefton MBC, UK) provided a dataset of beach transects at 139  
122 locations along the Morecambe Bay coastline, collected mostly between 2007 and 2022.

123



124

125 **Fig 1.** Location of data measurement sites (blue dots) along Morecambe coastline

126 The raw data from Sefton Council consisted of beach transects of varying lengths,  
 127 measured twice a year (spring and autumn) from 2007 and 2022 using GS16 Leica antenna  
 128 and Leica CS20 handset. The dataset was corrected in post processing using Lecia Infinity  
 129 software with an accuracy of Hz 3 mm + 0.1 ppm/ V 3.5 mm + 0.4 ppm. Locations with two  
 130 or fewer transects in time and those outside Morecambe Bay were discarded, leaving 125  
 131 locations with an average of 22 transects per location (Figure 1). Some of the transect had  
 132 varying length from year to year. To address this, the data were pre-processed and missed  
 133 datapoints were filled with the interpolated data from the three previous transects (e.g., if part  
 134 of the Autumn 2019 transect was missed, the missed section was filled through the average of  
 135 the 2019 (Summer) and 2018 (spring and autumn) values (see S1 for extended explanation  
 136 and table for this)). The raw data for all locations is available through Kumar and Leonardi  
 137 (2024b) and the raw data and interpolated transects are presented in supplementary file S1.  
 138 This interpolation was needed for around 20% of the transects (591 out of 2883). At few

139 locations, there were intervals in the transect data where measurements were taken with gaps  
140 in time. As presented in this file, these time gaps predominantly occurred in 2013 and 2015 at  
141 54 locations. Moreover, for 22 locations where the initial profile was measured in 2007, there  
142 was a significant gap between 2008 and 2012. After calculating the volume of sand at each  
143 location using the area under the curve method, which provided volumes in cubic meters per  
144 meter of beach width, the sediment volumes during these missing time gaps were interpolated  
145 using spline curves. For locations with notable time gaps between 2008 and 2012, the  
146 transects from 2007 and 2008 were excluded, enabling the transect time series to commence  
147 from 2012. A total of 256 profiles were interpolated to effectively complete the time series  
148 from 2010 to 2022 with two transects per year.

### 149 **3.2 Hydrodynamic modelling**

150 To obtain localized wave data, we simulated the hydrodynamic in Morecambe Bay  
151 using Delft3D. From the hydrodynamic model, we extracted wave height, wave velocity, and  
152 wave direction at each transect location. Details about the model setup and model validation  
153 can be found in Kumar et al., 2023a, b.

154 The model was calibrated using wave buoys at Morecambe Bay at Cleveleys and  
155 Heysham. To model realistic waves, we downloaded real-time wave data for the Cleveleys  
156 buoy station for the year 2022 from open source catalogue of coastal monitoring  
157 [https://www.coastalmonitoring.org/realtimedata/?chart=104&tab=download&disp\\_option=](https://www.coastalmonitoring.org/realtimedata/?chart=104&tab=download&disp_option=).

158 We applied this wave data to the sea boundary of the simulation domain. The model grid had  
159 a variable resolution, from 120×130 m onshore to 1000×300 m offshore. The simulation  
160 domain extended 57 km along the coastline and 20 km across, with a maximum distance from  
161 the sea boundary of 50 km. Wave and tide forcings were applied at the sea boundary, and a  
162 Neumann condition was applied at the lateral boundaries to allow wave energy to propagate  
163 freely. Real-time wave forcings were obtained from the Cleveleys buoy station for 2022. The  
164 model was run for 5 days, with a time step of 1 minute, from January 1st to 5th. Morphology

165 was not updated during the simulation, as the focus was on obtaining localized wave height,  
166 wave velocity, and wave direction. Modeling results were recorded every 10 minutes at  
167 observation points regularly spaced, at a distance of about 150 m, along the coastline and at a  
168 distance of about 500 m away from the starting point of beach transect measurement, which  
169 are usually on the landmass. This distance was chosen to ensure that the observation points  
170 are in the sea or in intertidal zone, allowing for a sufficient duration of water exposure for the  
171 collection of wave data. Most of the transects intersect with these observation points. The 125  
172 observation points nearest to each location were then selected from these observation points.

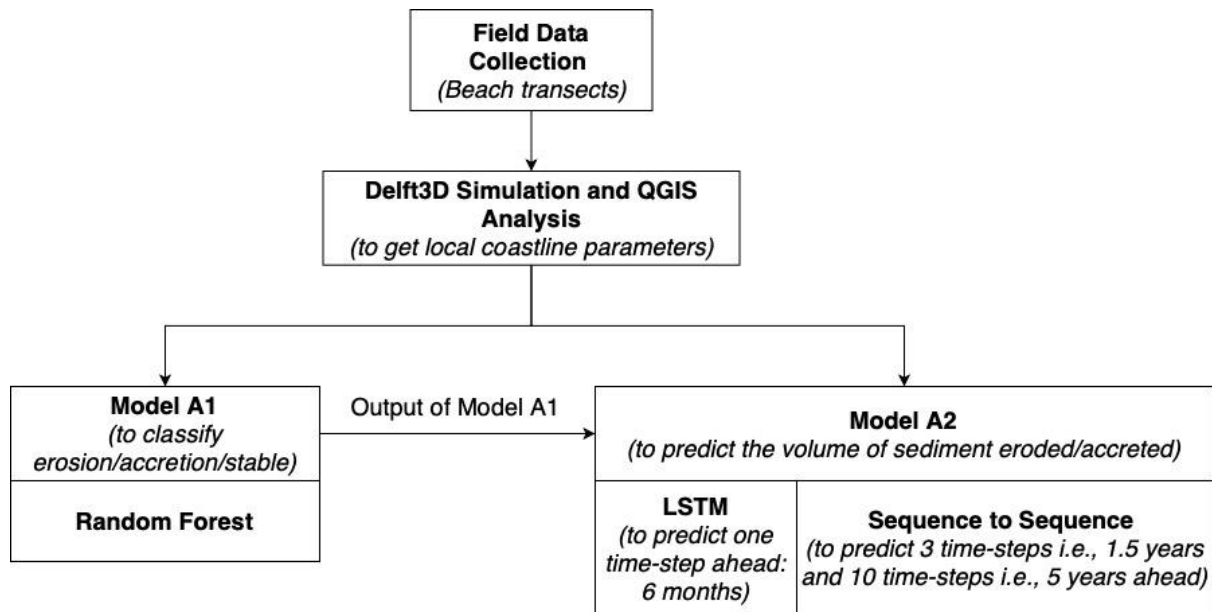
173 The coastline angle at each location was obtained using QGIS software, and the  
174 coastline was visually assessed using Google Earth based on vegetation presence to classify it  
175 as sandy, marshy (when vegetation is present across the whole transect), or marshy with  
176 mudflat. For some marsh areas, the length of transects were within the marshy area, so they  
177 were classified as marshy. For other locations, the length of transects were measured beyond  
178 the marshy areas into the mudflat, so they were classified as marshy with mudflat.

### 179 **3.3 Machine Learning modelling**

180 The preprocessed and simulation data were combined to match the selected 125  
181 locations and fed to the predictive models. Two predictive models were developed:

- 182 • Model A1 was developed to classify beach behavior as erosion, accretion, stable, or  
183 short-term fluctuation based on wave direction, wave velocity, coastline angle, and  
184 coastline composition.
- 185 • Model A2 to predict the available volume of sediment after erosion/accretion based on  
186 wave height, wave velocity, beach behavior (output of Model A1), and historical  
187 changes in sediment volume.

188 Model A1 is a random forest (RF) classifier. Model A2 is based on LSTM and sequence-  
189 to-sequence models. The methodology flowchart is presented in Figure 2.



190

191 **Fig 2.** Flow chart of methodology

192 **3.3.1 Model A1**

193 As shown in the methodology flowchart (Figure 2), field data and modelling data are  
 194 fed into Model A1, which classifies beach behavior as long-term erosion, accretion, stable or  
 195 short-term erosion fluctuation based on wave direction, wave velocity, coastline angle, and  
 196 coastline composition. A random forest (RF) classifier was used to classify beach behavior.  
 197 RF is a machine learning algorithm that builds an ensemble of decision trees to make  
 198 predictions. Decision trees are hierarchical classifiers that learn rules based on the values of  
 199 input variables. RF improves the performance of decision trees by averaging the predictions  
 200 of the trees, which reduces the variance of the model and makes it more robust to noise in the  
 201 data. RF can be used to solve both classification and regression problems. In classification  
 202 problems, the outcome is typically determined by the majority vote of the trees in the  
 203 ensemble, while in regression problems, the average of the predictions of the trees in the  
 204 ensemble is used. RF models are trained by resampling the training data using bootstrap  
 205 sampling (Pham et al., 2022; Wei et al., 2022) or bagging (Rodriguez-Galiano et al., 2015).  
 206 These methods create multiple training datasets by randomly sampling the original data with  
 207 or without replacement. Training each tree on a unique subset of the training data helps to

208 reduce the correlation between the trees (Rodriguez-Galiano et al., 2015). This is because  
209 some data points may be present in multiple subsets, while others may be excluded from all  
210 subsets. This reduced correlation makes the model more robust to variations in the input data  
211 and improves its predictive accuracy (Breiman, 2001).

212 The problem for this study was to train a RF model for multiclass classification on the  
213 MATLAB platform. Ensemble aggregation methods tried for this model were bagging,  
214 AdaBoostM2 (adaptive boosting for multiclass classification), LPBoost (linear programming  
215 boosting), RUSBoost (random undersampling boosting), and TotalBoost (totally collective  
216 boosting). Tree pruning was allowed based on the error. The number of trees tested was 50,  
217 75, and 100.

218 The inputs consisted of coastline angle (radian), wave direction (radian), and coastline  
219 composition (sandy, marshy, and marshy with mudflat), which was fed as categorical input.  
220 The target was classification of coastline behavior (long-term erosion, accretion, stable, and  
221 short-term erosion fluctuation), which was also fed as a categorical parameter. The output of  
222 Model A1 was used as input to Model A2 to provide a prediction of the available volume of  
223 sediment.

### 224 **3.3.2 Model A2**

225 To develop Model A2, we tested two models: LSTM and sequence-to-sequence (S2S),  
226 both of which were built using LSTM cells. LSTM is a type of recurrent neural network  
227 (RNN) that is commonly used for modeling time series data. LSTMs are designed to learn  
228 long-term dependencies in time series data by selectively storing important information and  
229 discarding unimportant information through different gates. These models were developed to  
230 address the problems associated with RNNs, which have difficulty learning long-term  
231 dependencies due to gradient explosion and gradient vanishing (Kumar et al., 2023;  
232 Lindemann et al., 2021; Sun et al., 2022). Unlike feed-forward neural networks (FFNNs),  
233 RNNs allow for feedback of data back to the hidden layers, which creates a time lag effect

234 that helps the model learn from previous time steps (Aslam et al., 2020). LSTM models can  
235 learn long-term dependencies in time series data using the gating mechanism in it. Kumar and  
236 Leonardi (2023a) provide a detailed discussion of the gating mechanism of LSTM models.

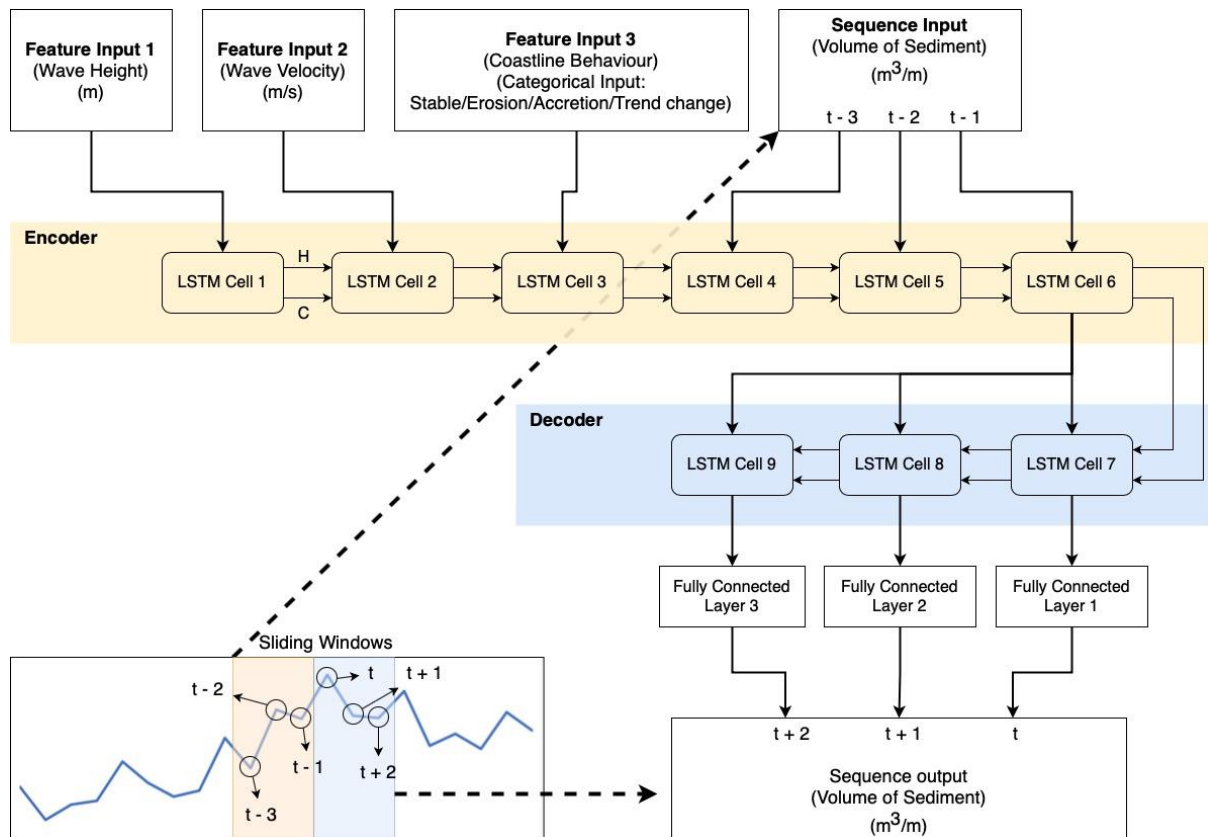
### 237 **3.3.2.1 LSTM model**

238 LSTM model was developed to predict sediment volume one time step ahead where each  
239 time step in the transect data corresponds to 6 months. The network consisted of a feature  
240 input layer, a sequence input layer, a sequence unfolding and folding layer, LSTM layers, and  
241 two fully connected layers followed by a regression layer. The feature input layer received  
242 feature inputs such as wave height, wave velocity, and coastline behavior (categorical). The  
243 sequence input layer received the previous three-time steps, equivalent to 1.5 years of  
244 sediment volume as its input. These feature and sequence inputs were combined at each time  
245 step using sequence unfolding and folding layer before feeding it to LSTM cells. The  
246 network was created and trained on a MATLAB platform. The number of LSTM layer tested  
247 were 3 and 4, each with 5, 10, 15, or 20 nodes. The cell weights were initialized using the He  
248 initializer. The cell state and hidden state of each layer were connected to the next layer in the  
249 sequence. This interconnection between cells allows LSTMs to capture and propagate  
250 information over time steps, which is crucial for modeling sequential data effectively.

### 251 **3.3.2.2 Sequence-to-Sequence (S2S)**

252 Sequence-to-Sequence (S2S) model S2S model was developed, in this study, to  
253 predict volume of sediment three-time step, i.e., 1.5 years, ahead based on the previous three-  
254 time step of volume of sediment time series and feature inputs. The S2S model consists of an  
255 encoder layer, which extracts information from the input data (Tang et al., 2016), and a  
256 decoder layer, which generates the output data based on the learned states (Kim et al., 2020).  
257 The encoder and decoder layers of the S2S model were implemented using LSTM layers  
258 (LSTM cell in figure 3), with 6 layers in the encoder and 3 layers in the decoder (Figure 3).  
259 All feature and sequence inputs, as discussed above for the LSTM model, were fed to the

260 corresponding LSTM layers of S2S model. The cell state (C) and hidden state (H) of each  
 261 layer were connected to the following layer in the network. The C, H, and output of the last  
 262 LSTM layer in the encoder were connected to the LSTM layers in the decoder, as shown in  
 263 figure 3. The output of each layer in the decoder was connected to regression layer, which  
 264 provided the output of the next three-time steps of sediment volume. The sequence input and  
 265 target were selected using the sliding window technique, as illustrated in Figure 3. Time steps  
 266  $t-3$ ,  $t-2$ , and  $t-1$  were used as input to predict time steps  $t$ ,  $t+1$ , and  $t+2$ . For the model  
 267 predicting 10-time step ahead, this network structure was extended by adding more LSTM  
 268 cells, along with their fully connected layer, in decoder to accommodate ten time steps from  $t$   
 269 to  $t+9$ . The number of nodes of each LSTM layers tested, in this study, varied from 5 to 50.  
 270 The model architecture was manually assembled, and its connections were managed  
 271 manually. The model was trained using a custom training loop on the MATLAB platform.



272

273 **Fig 3.** Model A2 structure

### 274 3.4. Performance criteria

275 This study utilizes both classification and regression models. The RF classifier  
276 performs multi-class classification between four categories, while the LSTM and S2S models  
277 perform regression prediction of time series. The prediction performance of both models is  
278 evaluated using different criteria. Accuracy, precision, recall, and F1 score were used to  
279 assess the performance of the RF classifier model, while regression mean absolute error  
280 (MAE) and Nash-Sutcliffe efficiency (NSE) were used to assess the performance of the  
281 LSTM and S2S models.

282 Accuracy measures the model's ability to correctly classify a given observation  
283 (equation 2). Precision measures the proportion of observations classified as positive by the  
284 model are actually positive (equation 3), indicating how reliable the model is for positive  
285 classifications. Recall measures the model's sensitivity by calculating the percentage of items  
286 actually present in the input that were correctly identified by the model (equation 4). F1 score  
287 measures the weighted harmonic mean of precision and recall scores (equation 5).

$$Accuracy = \frac{TP + TN}{TP + TN + FP + FN} \quad (2)$$

$$Precision = \frac{TP}{TP + FP} \quad (3)$$

$$Recall = \frac{TP}{TP + FN} \quad (4)$$

$$F_{\beta} = \frac{(\beta^2 + 1) * Precision * Recall}{\beta^2 * Precision + Recall} \quad (5)$$

288 where: TP = true positive i.e., positive observation correctly classified as positive; TN = true  
289 negative i.e., negative observation correctly classified as negative; FP = false positive i.e.,  
290 negative observation wrongly classified as positive; FN = false negative i.e., positive  
291 observation wrongly classified as negative;  $\beta$  is the weightage factor between precision and  
292 recall. For this study  $\beta = 1$  which gives equal weightage to the precision and recall, hence  $F_1$ .  
293 Equations 2, 3, 4, and 5 are designed for binary classifications, but this study involves multi-

294 class classification with four categories: erosion, accretion, stable, and short-term fluctuation.  
 295 When the model correctly classifies an erosion beach as erosion, it is considered as a true  
 296 positive. However, if the model classifies any other category as erosion, it is counted as a  
 297 false positive. This process applies to all four categories. In multi-class classification, a  
 298 weighted average approach is employed, where precision, recall, and F1 scores are calculated  
 299 for each category and then averaged weighting according to the number of samples in each  
 300 category present in the dataset.

301 The performance of regression models is evaluated using various metrics, including  
 302 regression (equation 6), MAE (equation 7), and NSE (equation 8). Regression provides a  
 303 statistical measure of how closely the predicted data aligns with the target data, indicating the  
 304 model's generalizing ability. MAE quantifies the error in the predicted values, while NSE  
 305 assesses the model's efficiency on a scale ranging from  $-\infty$  to 1, where 1 represents the most  
 306 efficient model.

$$r = \frac{n(\sum xy) - (\sum x)(\sum y)}{\sqrt{[n \sum x^2 - (\sum x)^2][n \sum y^2 - (\sum y)^2]}} \quad (6)$$

$$MAE = \frac{1}{n} \sum_{i=1}^n |x - y| \quad (7)$$

$$NSE = 1 - \frac{\sum (y - x)^2}{\sum (x - \bar{x})^2} \quad (7)$$

307 n is the number of data points, x is target value, y is predicted value

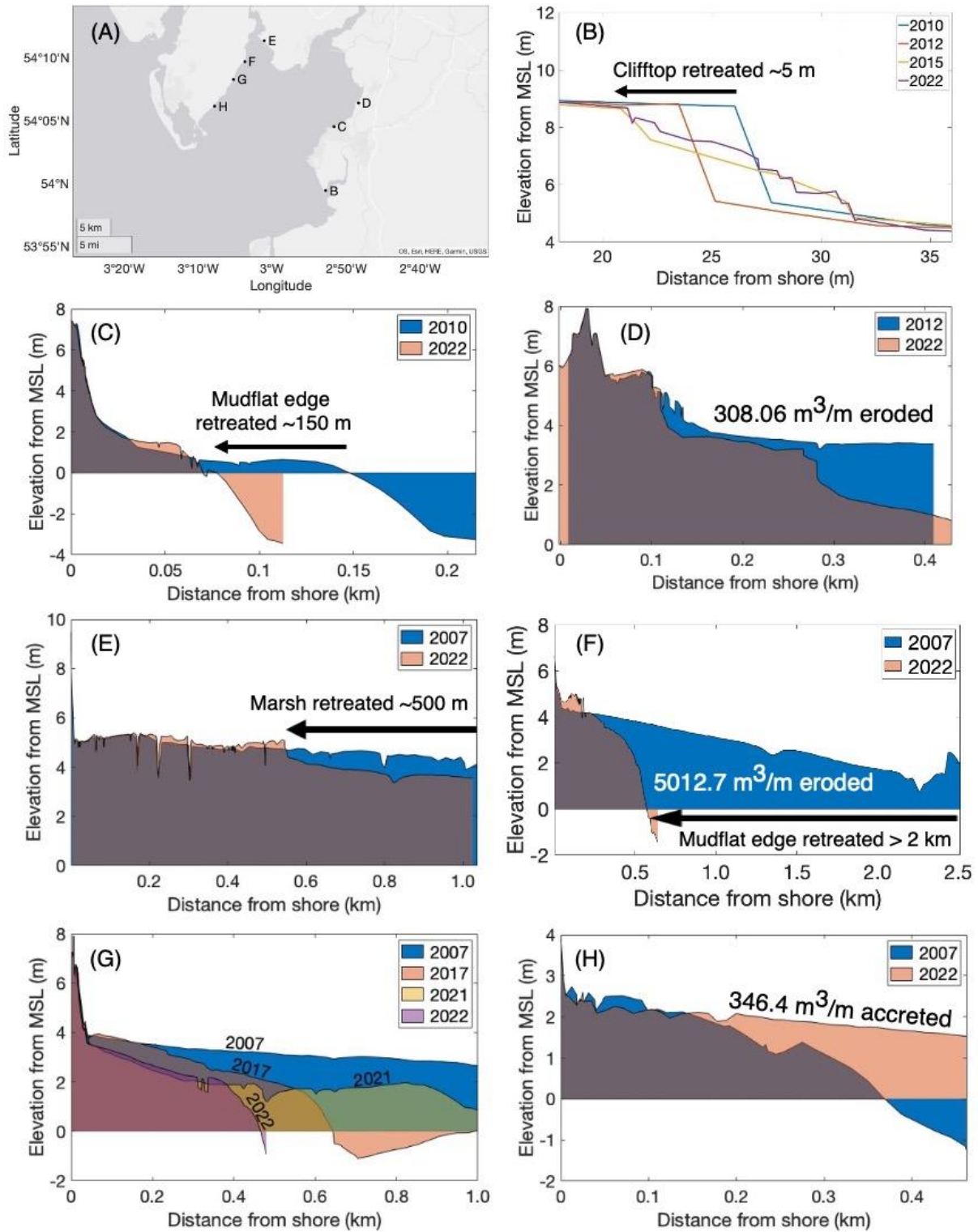
## 308 4. Results

### 309 4.1 Coastline analysis

310 Analysis of the data obtained from Sefton Council revealed rapid sediment movement  
 311 and instability along most part of the Morecambe Bay coastline. Marshy areas, mudflat edges  
 312 (defined as mudflat crossing zero mean sea level), and clifftops have retreated significantly,

313 indicating rapid coastal transformation. Sediment Volume changes indicate that only a  
314 minority of sites is stable.

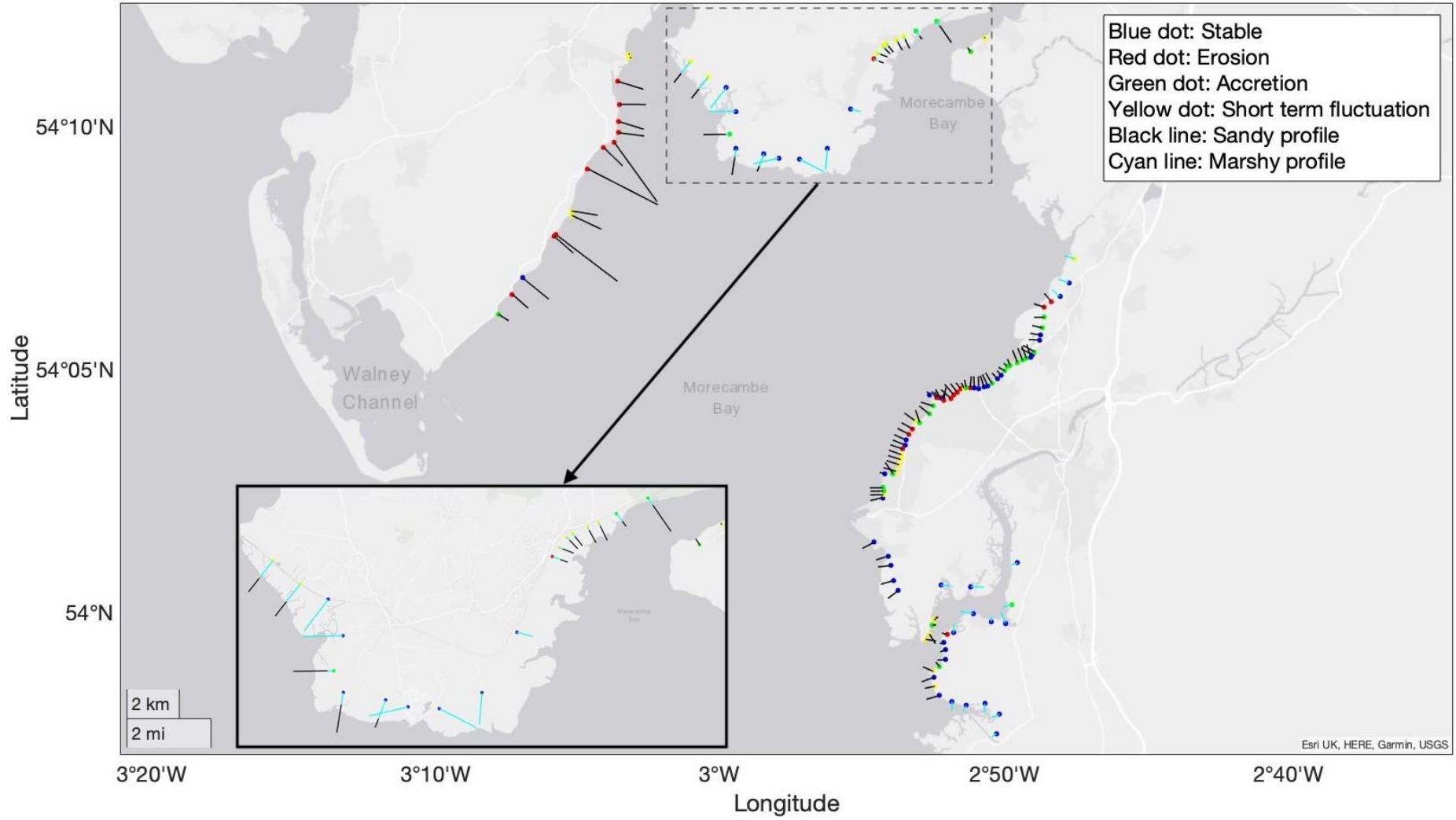
315 Figure 4 shows a selection of representative transects along Morecambe Bay for the  
316 stable, accreting, eroding and fluctuating cases. Figure 4B shows Sunderland Point in  
317 Morecambe, where according to our analysis the cliff top retreated about 5 meters between  
318 2010 and 2022. The first three profiles in Figure 4B (2010, 2012, and 2015) show significant  
319 retreat towards the landmass. As observed from Google Earth, rock armor was placed  
320 between 2013 and 2015, which reduced the retreat, as seen in its next profile in 2022. Figure  
321 4C and 4F show the transects experiencing mudflat edge retreat. Figure 4C shows transects  
322 near Morecambe city, where mudflat edge retreated about 150 m between 2010 and 2022.  
323 Figure 4F shows transects near Bardsea, where massive erosion of about  $5012.7 \text{ m}^3/\text{m}$   
324 sediment has caused the mudflat edge to retreat more than 2 kilometers between 2007 and  
325 2022. Figure 4D, near Morecambe city, shows significant erosion of  $308.06 \text{ m}^3/\text{m}$  of  
326 sediment between 2012 and 2022. Figure 4E shows transects near Ravenstown, a mostly  
327 marshy area that has experienced significant marshland loss in recent years. The location  
328 shown in Figure 4E has seen the marshland retreat about 500 meters between 2007 and 2022.  
329 Figure 4G shows short-term fluctuations in erosion between 2007 and 2022. The beach  
330 eroded between 2007 and 2017, accreted until 2021, and then eroded again in 2022. Figure  
331 4H shows transects between 2007 and 2022, which shows accretion of about  $346.4 \text{ m}^3/\text{m}$  of  
332 sediment resulting in the extension of mudflat edge towards the bay.



333

334 **Fig 4.** Beach profiles at different locations along Morecambe Bay coastline

335



336

337 **Fig 5.** Beach transects at different locations along Morecambe Bay coastline

338 Figure 5 shows the results of a transect analysis of all locations along the Morecambe  
339 Bay coastline. The length of each line represents the length of the transect measured at each  
340 location. Locations are classified as stable, eroding, accreting, or experiencing short-term  
341 fluctuations based on sediment volume changes at each location. Volume changes are  
342 calculated by subtracting the calculated sediment volume of each profile from the sediment  
343 volume of first profile measured in time.

344 This classification is indicated by different colored dots in Figure 5. Locations with  
345 less than 10% change in sediment volume are classified as stable. As shown in Figure 5, most  
346 marshy are classified as stable (blue). This is because transect length data is only available  
347 within marshy areas, where very little change is observed. Higher volume changes are  
348 noticeable for those transects extending to the mudflat and which are classified accordingly.  
349 For the remaining marshlands, transects extend beyond the marshland into the mudflat,  
350 recording sediment erosion from the mudflat and the retreat of the marshland. These  
351 classifications were fed to the prediction models (A1 and A2) to predict the volume of  
352 sediment available after erosion/accretion.

#### 353 **4.2 A1 model**

354 Model A1 was trained to classify beach behavior as eroding, accreting, stable, or  
355 undergoing short-term fluctuations based on four input parameters: coastline angle (radians),  
356 wave direction (radians), wave velocity (m/s), and transect type (categorical, e.g., marshy).  
357 The RF classifier model was tested using various ensemble aggregation methods (bagging,  
358 AdaBoostM2, LPBoost, RUSBoost, and TotalBoost) and different numbers of trees (50, 75,  
359 and 100). 15% of the data was reserved for testing, another 15% of the data was reserved for  
360 validation and the remaining 70% was used for training. These configurations yielded good  
361 prediction performance in terms of accuracy, precision, recall, and F1 score (table 1) with 75  
362 trees and RUSBoost method. This model effectively classifies beach behavior with training

363 accuracy of 0.95 and testing accuracy of 0.79, providing valuable input for Model A2's  
 364 prediction of sediment volume.

365 **Table 1.** Performance of A1 model

Criteria	Training	Testing
Accuracy	0.95	0.79
Precision	0.96	0.81
Recall	0.95	0.79
F1 Score	0.95	0.77

366

### 367 4.3 A2 model

368 Model A2 was developed to predict the available volume of sediment based on four  
 369 input parameters: wave height (m), wave velocity (m/s), coastline behavior (categorical  
 370 output from Model A1), and the previous 18 months (three-time steps) of sediment volume  
 371 ( $m^3/m$ ). Three models, one LSTM and two S2S, were evaluated for predicting 0.5 year (one  
 372 time step) ahead, 1.5 years (three time steps) and 5 years (ten time step) ahead, respectively.  
 373 For the LSTM model, three and four LSTM layers were tested. The number of nodes in the  
 374 LSTM layer was varied from 5 to 50. Ten percent of the data was reserved for testing, another  
 375 10% was used for validation, and the remaining 80% was used for training. Both models  
 376 demonstrated remarkable accuracy in predicting available sediment volume (table 2). The  
 377 LSTM model achieved excellent accuracy when tested with four LSTM layers and 20 nodes  
 378 in each layer, while the two S2S models achieved excellent accuracy with 50 and 40 nodes in  
 379 its LSTM layers for predicting 1.5 and 5 years ahead, respectively.

380 **Table 2.** Performance of A2 model

Model	Phase	Regression	MAE ( $m^3/m$ )	NSE
LSTM	Training	0.9966	0.0504	0.9929
	Testing	0.9961	0.0567	0.9915
S2S	Training	0.9967	0.0491	0.9933

(1.5 years)	Testing	0.9950	0.0552	0.9900
S2S	Training	0.9951	0.0645	0.9900
(5 years)	Testing	0.9916	0.0656	0.9828

381

382           The S2S models predict multiple time-step values simultaneously, with Table 2  
383 presenting the average accuracy across individual time steps. A detailed breakdown of  
384 accuracy reveals testing MAE values for t, t+1, and t+2 at 0.0434, 0.0567, and 0.0656,  
385 respectively, for a 1.5-year prediction. For a 5-year prediction, testing MAE values are listed  
386 as 0.0481, 0.0597, 0.0625, 0.0607, 0.0647, 0.0615, 0.0692, 0.0712, 0.0736, and 0.0851 m<sup>3</sup>/m.  
387 Notably, the accuracy for the first-time step is lower than that of the LSTM model, which is  
388 tailored for single-step prediction. The S2S models exhibit a decreasing accuracy trend,  
389 indicating an increasing error as the number of predicted time steps increases. While the  
390 LSTM model excels at one-step prediction, the S2S model is recommended for longer  
391 predictions. However, it's essential to consider the escalating error in later time steps when  
392 utilizing the S2S approach.

393 **Discussion**

394           Coastline changes in Morecambe Bay have been observed and studied since 1990s by  
395 several researchers including Pringle (1995), Mason et al. (1999) and Mason et al. (2010).  
396 These studies have documented significant changes in the bathymetry near the coastline.  
397 Pringle (1995) noticed the erosion of salt marshes, which began in mid-1970s and continued  
398 into the 1990s at a relatively slow rate. In addition to the erosion of salt marshes, the Kent  
399 channel of Morecambe also shifted eastward along with its minor channels during the late  
400 1970s, leading to rapid saltmarsh erosion. Mason et al. (1999), observed the movement of the  
401 Leven estuary of Morecambe towards the north-east by about 2 km during the period of  
402 1992-1997. Mason et al. (2010) also observed the migration of the Ulverston channel of

403 Morecambe north-east by about 5 km between 1991 to 2004. Similarly, this study, conducted  
404 with the data between 2007 and 2022, also observed significant erosion of mudflat platforms  
405 and marshy regions in most parts of Morecambe. This erosion has resulted in the mudflat  
406 edges, i.e., zero mean sea level crossing of mudflats, retreating up to 2 kilometers (crossing of  
407 mean sea level) and marshes up to 500 meters towards the landmass (figure 4). These  
408 dynamic changes in bathymetry near the coastline pose significant challenges for the  
409 infrastructure sector and coastal communities.

410 The models developed in this study can effectively identify erosion hotspots and  
411 predict sediment volume changes based on simplified modelling and QGIS inputs. Model A1  
412 is designed to classify the coastline behavior as eroding, accreting, stable or undergoing short  
413 term fluctuations based on inputs of coastline angle, wave velocity, wave direction and  
414 coastline composition. Model A2 is specifically designed to estimate the volume of sediment  
415 eroded or accreted along the coastline based on inputs of wave height, wave velocity,  
416 coastline behavior (output from Model A1), and the previous 18 months of sediment volume  
417 and at a time scale of 1.5 years and 5 years.

418 These models have the advantage of providing highly accurate predictions for  
419 Morecambe Bay, as they are trained on a comprehensive field dataset from Morecambe Bay.  
420 While their accuracy may decrease when applied to other embayments, they can still be  
421 effectively utilized in areas with similar coastal dynamics and wave conditions to Morecambe  
422 Bay. The advantage of this methodology lies in its development of two predictive models.  
423 One of these models (model A1) is dedicated to identifying erosion hotspots, critical  
424 information for effective coastline management. According to a report by Masselink et al.  
425 (2020), 17.3% of the UK coastline, equivalent to 3008 km, is currently experiencing erosion.  
426 The report further notes that only 45.6% of England's coastline is protected by coastal  
427 defense structures such as groynes, seawalls, or artificial beaches. Model A1 can be utilized

428 to pinpoint erosive locations along the coastlines, facilitating targeted deployment of coastal  
429 defense measures to protect vulnerable areas. Additionally, this model feeds its output into  
430 the second model (model A2), enabling the latter to learn beach classification—whether  
431 eroding, accreting, fluctuating, or stable—and subsequently predict sediment volumes in the  
432 future. Accurately estimating sediment losses from various beaches, including cliff beaches  
433 (as discussed by Brooks and Spencer (2010)), holds regional significance as these sediments  
434 play crucial roles in beach maintenance, nearshore bank systems, and nearshore sediment  
435 transport pathways. Model A2 can thus be applied to forecast sediment erosion volumes  
436 along beaches, thereby assisting in better understanding and managing coastal erosion  
437 processes and their impacts on coastal ecosystems and communities.

438 Another advantage of using ANN models are that these are computationally  
439 inexpensive (Hashemi et al., 2010), as compared to the simulation models which typically  
440 require hours for simulation. Thus, the sediment volume change can be predicted instantly in  
441 the scale of 5 years. A drawback of ANN, as suggested by Hashemi et al. (2010), is that its  
442 prediction accuracy is depended on quality of data. However, this study has the advantage of  
443 training models on high quality field data.

444 Additionally, these models are trained to forecast data points three and ten steps ahead  
445 in the time series, equivalent to 1.5 and 5 years into the future respectively, using only 18  
446 months of historical sediment volume data. The prediction performance was evaluated across  
447 two different time scales to assess the model's ability to forecast over longer durations. For a  
448 5-year forecast, the model demonstrates high accuracy with a testing regression of 0.9916.  
449 However, upon analyzing the ten individual time steps, an increasing error trend becomes  
450 apparent. The MAE rises from 0.0481 m<sup>3</sup>/m for the first-time step to 0.0851 m<sup>3</sup>/m for the  
451 tenth time step, nearly doubling from the initial prediction. Nevertheless, the prediction error

452 for the tenth time step remains within acceptable bounds, supported by a testing regression of  
453 0.9878.

454 Future developments of these models will involve incorporating additional historical  
455 data, enabling the models to scale up and provide forecasts for even longer time horizons.  
456 Moreover, enhancing the input list with additional features is certain to enhance prediction  
457 capabilities by enabling models to grasp the relationship between coastal erosion and various  
458 variables. As demonstrated by Peponi et al. (2019), factors such as urbanization and  
459 population influence coastal dynamics systems by modifying hydrological patterns,  
460 sedimentation regimes, land use and land cover. Additionally, coastal erosion is influenced by  
461 rising sea levels (Masselink et al., 2020). Thus, incorporating these factors into the model's  
462 input list will facilitate learning the relationship between sediment erosion along the coastline  
463 and these variables, ultimately enhancing the model's predictive robustness.

#### 464 **Conclusion**

465 This study analyzes field data comprising beach transects at 125 locations along the  
466 Morecambe Bay coastline. The analysis reveals areas of rapid coastal change. Following the  
467 data analysis, this study investigates the potential of a two-stage machine learning model for  
468 predicting sediment volume change in a coastal environment. The model utilized a  
469 combination of beach behavior classification and deep learning techniques to achieve  
470 accurate predictions. The results demonstrated that the model effectively captured the  
471 complex relationship between beach behavior, wave conditions, and sediment erosion and  
472 accretion.

473 Model A1 successfully classified beach behavior into four categories: eroding, accreting,  
474 stable, and undergoing short-term fluctuations using Random Forests and based on input of  
475 coastline angle, wave velocity, wave direction and coastline composition. This classification  
476 provided valuable input for Model A2, which utilized LSTM and sequence-to-sequence

477 models to predict available sediment volume for one-step-ahead and multi-step-ahead  
478 predictions, respectively. The LSTM model achieved a testing regression of 0.9961 for one-  
479 step-ahead (6 months) predictions of available sediment volume time series, while the  
480 sequence-to-sequence models achieved a testing regression of 0.9950 for three-time-step-  
481 ahead (1.5 years) predictions and 0.9916 for ten-time-steps (5 years) prediction. Proposed  
482 models offer several advantages over traditional time series models. Firstly, it explicitly  
483 classifies beach behavior based on input of coastline angle, wave velocity, wave direction,  
484 and coastline composition. Secondly, the model is highly generalizable and can be applied to  
485 different coastal environments with minimal adjustments.

#### 486 **Acknowledgement**

487 We acknowledge the following funding source for this study: Engineering with Nature:  
488 combining Artificial intelligence, Remote sensing and computer Models for the optimum  
489 design of coastal protection schemes EP/V056042/1. We acknowledge Paul Wisse, Samantha  
490 Godfrey-Lord, Andrew Martin and Michelle Barnes from Sefton Council for providing data  
491 from the coastal monitoring program.

#### 492 **Open Research:**

#### 493 **Data Access Statement:**

494 The data obtained from the Sefton Council for this study is available through Kumar and  
495 Leonardi (2024b).

496

#### 497 **References:**

- 498 Adamo, F., De Capua, C., Filianoti, P., Lanzolla, A. M. L., & Morello, R. (2014). A coastal  
499 erosion model to predict shoreline changes. *Measurement*, *47*, 734-740.  
500 doi:<https://doi.org/10.1016/j.measurement.2013.09.048>
- 501 Anctil, F., Fillion, M., & Tournebize, J. (2009). A neural network experiment on the  
502 simulation of daily nitrate-nitrogen and suspended sediment fluxes from a small  
503 agricultural catchment. *Ecological Modelling*, *220*(6), 879-887.  
504 doi:10.1016/j.ecolmodel.2008.12.021
- 505 Aslam, M., Lee, J.-M., Kim, H.-S., Lee, S.-J., & Hong, S. (2020). Deep Learning Models for  
506 Long-Term Solar Radiation Forecasting Considering Microgrid Installation: A  
507 Comparative Study. *energies*, *13*(1). doi:10.3390/en13010147
- 508 Betzold, C., & Mohamed, I. (2017). Seawalls as a response to coastal erosion and flooding: a  
509 case study from Grande Comore, Comoros (West Indian Ocean). *Regional*  
510 *Environmental Change*, *17*(4), 1077-1087. doi:10.1007/s10113-016-1044-x
- 511 Breiman, L. (2001). Random forests. *Machine learning*, *45*, 5-32.
- 512 Brooks, S. M., & Spencer, T. (2010). Temporal and spatial variations in recession rates and  
513 sediment release from soft rock cliffs, Suffolk coast, UK. *Geomorphology*, *124*(1), 26-  
514 41. doi:<https://doi.org/10.1016/j.geomorph.2010.08.005>

- 515 Browder, A. E., Dean, R. G., & Chen, R. (2015). Performance of a Submerged Breakwater  
516 for Shore Protection. In *Coastal Engineering 1996* (pp. 2312-2323).
- 517 Corbella, S., & Stretch, D. D. (2012). Predicting coastal erosion trends using non-stationary  
518 statistics and process-based models. *Coastal Engineering*, 70, 40-49.  
519 doi:<https://doi.org/10.1016/j.coastaleng.2012.06.004>
- 520 Crawford, T. W., Islam, M. S., Rahman, M. K., Paul, B. K., Curtis, S., Miah, M. G., & Islam,  
521 M. R. (2020). Coastal Erosion and Human Perceptions of Revetment Protection in the  
522 Lower Meghna Estuary of Bangladesh. *Remote Sensing*, 12(18).  
523 doi:10.3390/rs12183108
- 524 Farzad, F., & El-Shafie, A. H. (2017). Performance Enhancement of Rainfall Pattern – Water  
525 Level Prediction Model Utilizing Self-Organizing-Map Clustering Method. *Water*  
526 *Resources Management*, 31(3), 945-959. doi:10.1007/s11269-016-1556-7
- 527 Harris, L. E. (2012). Submerged Reef Structures for Beach Erosion Control. In *Coastal*  
528 *Structures 2003* (pp. 1155-1163).
- 529 Hashemi, M. R., Ghadampour, Z., & Neill, S. P. (2010). Using an artificial neural network to  
530 model seasonal changes in beach profiles. *Ocean Engineering*, 37(14), 1345-1356.  
531 doi:<https://doi.org/10.1016/j.oceaneng.2010.07.004>
- 532 Kim, J., Yun, J.-H., & Kim, H. C. (2020, 2020/). *Anomaly Detection for Industrial Control*  
533 *Systems Using Sequence-to-Sequence Neural Networks*. Paper presented at the  
534 Computer Security, Cham.
- 535 Kumar, P., Ahmed, A. N., Sherif, M., Sefelnasr, A., & Elshafie, A. (2023). Development of  
536 Long Short-Term Memory Model for Prediction of Water Table Depth in United Arab  
537 Emirates. In M. Sherif, V. P. Singh, A. Sefelnasr, & M. Abrar (Eds.), *Water Resources*  
538 *Management and Sustainability: Solutions for Arid Regions* (pp. 141-152). Cham:  
539 Springer Nature Switzerland.
- 540 Kumar, P., & Leonardi, N. (2023a). Exploring Mega-Nourishment Interventions Using Long  
541 Short-Term Memory (LSTM) Models and the Sand Engine Surface MATLAB  
542 Framework. *Authorea*. doi:<https://doi.org/10.22541/au.169297181.19761587/v1>
- 543 Kumar, P., & Leonardi, N. (2023b). A novel framework for the evaluation of coastal  
544 protection schemes through integration of numerical modelling and artificial  
545 intelligence into the Sand Engine App. *Scientific Reports*, 13(1), 8610.  
546 doi:10.1038/s41598-023-35801-5
- 547 Kumar, P., & Leonardi, N. (2024a). Exploring Mega-Nourishment Interventions Using Long  
548 Short-Term Memory (LSTM) Models and the Sand Engine Surface MATLAB  
549 Framework. *Geophysical Research Letters*, 51(4), e2023GL106042.  
550 doi:<https://doi.org/10.1029/2023GL106042>
- 551 Kumar, P., & Leonardi, N. (2024b). *High-Resolution Beach Profile Time Series: Morecambe*  
552 *Bay, [Dataset]. Zenodo.2007-2022*. <https://doi.org/10.5281/zenodo.10907660>.
- 553 Lima, M., Coelho, C., Veloso-Gomes, F., & Roebeling, P. (2020). An integrated physical and  
554 cost-benefit approach to assess groins as a coastal erosion mitigation strategy. *Coastal*  
555 *Engineering*, 156, 103614. doi:<https://doi.org/10.1016/j.coastaleng.2019.103614>
- 556 Lindemann, B., Maschler, B., Sahlab, N., & Weyrich, M. (2021). A survey on anomaly  
557 detection for technical systems using LSTM networks. *Computers in Industry*, 131,  
558 103498. doi:<https://doi.org/10.1016/j.compind.2021.103498>
- 559 Mason, D. C., Amin, M., Davenport, I. J., Flather, R. A., Robinson, G. J., & Smith, J. A.  
560 (1999). Measurement of Recent Intertidal Sediment Transport in Morecambe Bay  
561 using the Waterline Method. *Estuarine, Coastal and Shelf Science*, 49(3), 427-456.  
562 doi:<https://doi.org/10.1006/ecss.1999.0508>
- 563 Mason, D. C., Scott, T. R., & Dance, S. L. (2010). Remote sensing of intertidal  
564 morphological change in Morecambe Bay, U.K., between 1991 and 2007. *Estuarine*,

- 565 *Coastal and Shelf Science*, 87(3), 487-496.  
 566 doi:<https://doi.org/10.1016/j.ecss.2010.01.015>
- 567 Masselink, G., Russell, P., Rennie, A., Brooks, S., & Spencer, T. (2020). Impacts of climate  
 568 change on coastal geomorphology and coastal erosion relevant to the coastal and  
 569 marine environment around the UK. *MCCIP Science Review*, 2020, 158-189.
- 570 Peponi, A., Morgado, P., & Trindade, J. (2019). Combining Artificial Neural Networks and  
 571 GIS Fundamentals for Coastal Erosion Prediction Modeling. *Sustainability*, 11(4).  
 572 doi:10.3390/su11040975
- 573 Pham, Q. B., Kumar, M., Di Nunno, F., Elbeltagi, A., Granata, F., Islam, A. R. M. T.,  
 574 Talukdar, S., Nguyen, X. C., Ahmed, A. N., & Anh, D. T. (2022). Groundwater level  
 575 prediction using machine learning algorithms in a drought-prone area. *Neural  
 576 Computing and Applications*, 34(13), 10751-10773. doi:10.1007/s00521-022-07009-7
- 577 Prasad, D. H., & Kumar, N. D. (2014). Coastal Erosion Studies<sup>o</sup>™A Review. *International  
 578 Journal of Geosciences*, Vol.05No.03, 5. doi:10.4236/ijg.2014.53033
- 579 Pringle , A. W. (1995). Erosion of a cyclic saltmarsh in Morecambe Bay, North-West  
 580 England. *Earth Surface Processes and Landforms*, 20(5), 387-405.  
 581 doi:<https://doi.org/10.1002/esp.3290200502>
- 582 Rodriguez-Galiano, V., Sanchez-Castillo, M., Chica-Olmo, M., & Chica-Rivas, M. (2015).  
 583 Machine learning predictive models for mineral prospectivity: An evaluation of neural  
 584 networks, random forest, regression trees and support vector machines. *Ore Geology  
 585 Reviews*, 71, 804-818. doi:<https://doi.org/10.1016/j.oregeorev.2015.01.001>
- 586 Sharma, V., Negi, S. C., Rudra, R. P., & Yang, S. (2003). Neural networks for predicting  
 587 nitrate-nitrogen in drainage water. *Agricultural Water Management*, 63(3), 169-183.  
 588 doi:10.1016/s0378-3774(03)00159-8
- 589 Sun, J., Hu, L., Li, D., Sun, K., & Yang, Z. (2022). Data-driven models for accurate  
 590 groundwater level prediction and their practical significance in groundwater  
 591 management. *Journal of Hydrology*, 608, 127630.  
 592 doi:<https://doi.org/10.1016/j.jhydrol.2022.127630>
- 593 Tang, Y., Xu, J., Matsumoto, K., & Ono, C. (2016, 12-15 Dec. 2016). *Sequence-to-Sequence  
 594 Model with Attention for Time Series Classification*. Paper presented at the 2016 IEEE  
 595 16th International Conference on Data Mining Workshops (ICDMW).
- 596 van Rijn, L. C. (2011). Coastal erosion and control. *Ocean & Coastal Management*, 54(12),  
 597 867-887. doi:<https://doi.org/10.1016/j.ocecoaman.2011.05.004>
- 598 Wei, A., Chen, Y., Li, D., Zhang, X., Wu, T., & Li, H. (2022). Prediction of groundwater level  
 599 using the hybrid model combining wavelet transform and machine learning  
 600 algorithms. *Earth Science Informatics*, 15(3), 1951-1962. doi:10.1007/s12145-022-  
 601 00853-0
- 602 Williams, A. T., Rangel-Buitrago, N., Pranzini, E., & Anfuso, G. (2018). The management of  
 603 coastal erosion. *Ocean & Coastal Management*, 156, 4-20.  
 604 doi:<https://doi.org/10.1016/j.ocecoaman.2017.03.022>

605